Continuous order-disorder phase transitions of the $p(2\times2)$ and $(\sqrt{3}\times\sqrt{3})R30°$ superstructures of sulfur on Ru(001): Effective critical exponents and finite size effects

M. Sokolowski*
Physikdepartment E20, Technische Universität München, James Franck Straße, D-85747 Garching, Germany

H. Pfnür
Institut für Festkörperphysik, Universität Hannover, Appelstraße 2, D-30167 Hannover, Germany
(Received 27 September 1993)

Critical properties of the two-dimensional order-disorder phase transitions of the $p(2\times2)$ and the $(\sqrt{3}\times\sqrt{3})R30°$ superstructures of sulfur chemisorbed on Ru(001) were determined by spot-profile analysis using high-resolution low-energy electron diffraction. Both transitions are continuous, as evident from the power-law behavior observed for $0.01 \leq |t| \leq 0.1$ ($t = T/T_c - 1$) and from the values obtained for the criticial exponents. For smaller $|t|$ the phase transitions are finite-size rounded by an interaction of the superstructure domains with steps (average distance between steps ~275 Å). The values of the effective exponents β of the order parameter, ν of the correlation length, γ of the susceptibility and the exponent η [only determined for p(2×2)] fall close to the values theoretically predicted for the four-state and three-state Potts universality classes, respectively. Deviations of experimental values from Potts values, found for β and γ, are attributed to corrections to scaling which in part might be specific to the lattice gas. Additional experiments on vicinal surfaces with higher step densities show that pinning of the superstructure domains at monoatomic steps limits the correlation length to values below the average terrace width. The finite-size-induced effects are quantitatively compatible with predictions from finite-size scaling theory.

INTRODUCTION

Continuous phase transitions in two dimensions (2D) have been a matter of growing interest in experimental and theoretical studies over the past ten years since critical fluctuations play a more important role in lower dimensions and significant deviations of critical exponents from Landau's classical mean field exponents are expected. For the experimental study of 2D phase transitions, chemisorbed layers on high symmetry crystal surfaces in the submonolayer coverage regime are attractive test systems because lattice-gas-type superstructures with only one specific adsorption site populated are formed in many cases. Using symmetry arguments the order-disorder phase transitions of such superstructures can be classified and grouped into universality classes.[1] Remarkably, there are only very few universality classes in 2D which exhibit continuous phase transitions,[1,2] among which the Ising ($q = 2$), the three-state and four-state Potts models ($q = 3$ and 4), respectively and the XY model with cubic anisotropy are the most important. Experimental verifications for these universality classes can be found by order-disorder phase transitions in adsorbed layers. A relatively small number of experiments using diffraction techniques has been reported in the literature.[3–5] Often a general understanding of the experimental situation is only possible by help of computational studies using Monte Carlo simulations (MCS) on lattice-gas models.[5] In addition, studies of phase diagrams of adsorbed layers are a major source of information about the lateral interactions between the adsorbed particles which can be obtained from a comparison of the experimental phase diagrams with MCS model calculations.[6]

In this work we report an experimental analysis of the critical properties of the order-disorder phase transitions of the $p(2\times2)$ and $(\sqrt{3}\times\sqrt{3})R30°$ superstructures of atomic sulfur adsorbed on the Ru(001) base plane using low-energy electron diffraction (LEED). This system is of interest since both transitions can be continuous according to the "Landau rules,"[1] and they actually are, as will be shown below. In this case, the critical behavior of the $p(2\times2)$ and the $(\sqrt{3}\times\sqrt{3})R30°$ phase transitions is expected to fall into the four-state and the three-state Potts universality classes, respectively.[1] Therefore, this system allows a direct comparison of two continuous phase transitions of superstructures with different symmetries in 2D. For the $\sqrt{3}$ structure, our results represent experimental verification of critical exponents in the three-state Potts universality class for a chemisorbed system.

Experimentally, the quantitative determination of critical behavior and exponents requires data over a sufficient range in reduced temperature, $t = (T - T_c)/T_c$ (T_c is the critical temperature), close to the phase transition. This is not easy to obtain because close to the phase transition the length scale of the fluctuations, i.e., the correlation length ξ, becomes very large and causes an extreme sensitivity to surface defects such as point defects and steps. This limits the range in t where critical behavior can be observed, even for well prepared surfaces, as we will demonstrate. In the simplest case, i.e., if the

defects such as steps limit the length over which fluctuations are correlated, finite-size rounding is expected. On the other hand, if the lateral interactions in the adsorbate are strong enough that the correlations persist across step edges no finite-size effects due to the steps are observed. Instead, the overall symmetry of the system is lowered and the critical exponents can be changed. This situation was found recently by us for $p(2\times2)$-ordered oxygen on Ru(001).[7,8] Explicit vectors connecting oxygen atoms on different terraces across monoatomic steps can be given[9] using the phase information from a LEED-IV study for profile simulation of split superstructure profiles. Whereas on the flat surface the order-disorder phase transition of this structure is continuous with experimental exponents in the four-state Potts universality class, exponents change to Ising-like values on stepped surfaces.[8]

For sulfur on Ru(001), the influence of imperfections of the sample turns out to be very different from that found for oxygen. Here the monoatomic steps limit the range of correlations to single terraces and reduce the temperature range where power-law behavior can be observed. Nevertheless, the determination of critical exponents is still possible with reasonable accuracy. Because of the limited temperature range of one order of magnitude for the determination of the critical exponents, we cannot separate corrections to scaling from our data. The determined exponents therefore have to be considered as *effective* exponents.[10] As we will show, deviations from the critical behavior of the Potts universality classes are observed for both transitions, indicating that there are indeed corrections present, which are probably enhanced due to the lattice-gas character of the phase transitions.

The influence of finite-size effects on 2D phase transitions on surfaces has been studied only in a small number of experiments so far, mainly with physisorbed adsorbates or with reconstructions of clean surfaces.[11,12] In contrast, variation of system size is a common method in MCS.[13] Therefore, there is also strong interest in experimental data. Since the correlation length is limited by steps and can be controlled by the step distance for S/Ru(001), this chemisorbed system offers the possibility to investigate finite-size effects systematically. For this purpose, we have performed experiments on two vicinal surfaces with well defined increased step densities in addition to the experiments on a surface with small step density. The data of the $p(2\times2)$ phase transition on the different surfaces were then compared for the different step densities. Indeed, we observed that the finite-size rounding is in accordance with the finite size scaling hypothesis.

This work is organized as follows. We start with the description of the experimental setup and the characterization of the nominally flat surface followed by a description of the relevant section of the S/Ru(001) phase diagram. The analysis of the critical behavior of $p(2\times2)$ and $(\sqrt{3}\times\sqrt{3})R30°$ phase transitions and the determination of the effective critical exponents forms the main part of the present work. It is supplemented by experiments on vicinal surfaces. We close with a discussion and a summary.

EXPERIMENT

The experiments were performed in a standard UHV chamber (base pressure 2×10^{-11} mbar) with a double μ metal shielding. The Ru samples were cut by spark erosion from a Ru single crystal of 99.99% purity, oriented to better than 0.5° by Laue diffraction and polished with diamond pastes down to 0.25 μm grain size. The samples were cleaned in ultrahigh vacuum by extensive temperature cycles in oxygen. Three different surfaces were prepared. The first was cut in the (001) plane and is termed as the *nominally flat* surface in this work. Two *vicinal* surfaces were prepared with tilt angles of 4.0° and −1.8° with respect to the (001) plane and the direction of steps chosen along the close-packed rows ($\overline{\Gamma K}$ direction). The average terrace widths were 33 Å and 85 Å, respectively. Details of the vicinal surfaces can be found in Ref. 9; those of the nominally flat surface are reported below.

The computerized temperature control had a resolution of 0.1 K and allowed temperature ramping linear in time.[14] The sample was cooled with liquid N_2 and heated by direct current through its mounting. The mounting consisted of two tungsten wires spot welded to the back of the sample. For LEED measurements the heating current was chopped with 12.5 Hz. Diffracted electrons were detected only during off times of the heating current. As temperature dropped during the measuring intervals, an effective averaging of temperatures took place over 0.4 K at most. Further apparative details are described in Ref. 7. LEED profile measurements were carried out using a high-resolution LEED instrument (SPALEED) with a nominal transfer width of 1200 Å.[15] In addition, intensities integrated over the diffraction spots were measured versus temperature using a Faraday-cup instrument with low angular resolution.

Sulfur was dosed using an electrochemical $Ag_2S/AgI/Ag$ cell which primarily emits S_2. For details see Ref. 16. For fine tuning of the coverage, parts of the layer were either desorbed or the sample was exposed to small amounts of H_2S in addition. Heating to more than 1000 K causes slow diffusion of S into the bulk. S segregates back to the surface close to room temperature. Care was taken, monitoring T_c versus time, that changes in coverage due to this effect were less than 0.001 monolayer per hour for relevant measurements. For quantitative evaluations one-dimensional cuts through first order superstructure beams were measured in the symmetry directions $\overline{\Gamma M}$ and $\overline{\Gamma K}$ as well as in the $\overline{MK}$ directions normal to these at 100 eV beam energy. In addition, peak intensities versus temperature curves were measured at heating rates between 0.2 and 2 K/s. Peak intensities, integrated intensities, and profiles were found to be fully reversible in all cases considered in this paper with no hysteresis detectable.

SURFACE MORPHOLOGY

In order to characterize the surface morphology of the nominally flat surface, one-dimensional cuts through the specular (0,0) spot were taken as a function of k_z, i.e.,

the component of the scattering vector **k** perpendicular to the surface, by variation of the beam energy. The full width at half maximum (FWHM) of profiles for two perpendicular scan directions are plotted versus k_z in Fig. 1. Both data sets show an approximately linear increase with k_z with pronounced equidistant oscillations due to *monoatomic* steps on the surface. The minima of the oscillations are found at energies where all terraces of the surface scatter in phase, i.e., where $k_z d = n\,2\pi$, d being the height of the steps on the surface. Since the amplitude of the oscillations depends systematically on the scan direction, the steps must be preferentially oriented, and thus the macroscopic surface is slightly vicinal to the (001) plane due to a small accidental misorientation during the preparation. From the amplitude ($\frac{1}{2}\Delta k_z$) of the oscillations we estimate the FWHM Δk_z of the spot profiles at the antiphase conditions and thus the average terrace width $\Lambda = 2\pi/\Delta k_z$ of (275 ± 50) Å, which corresponds to a miscut angle of 0.5°. Since the terrace-width distribution is not fully known, the correct value for Λ might differ from the estimated value by a factor of the order of one.[17] Nevertheless, this uncertainty should not be a source of major error in the further analysis since absolute values for correlation lengths (see below) are derived from the inverse FWHM of spot profiles in the same manner. The direction of the step edges was determined from the direction of maximum splitting to be 10° off the $\overline{\Gamma K}$-direction.

The general linear increase of the FWHM with k_z in Fig. 1 is due to the mosaic spread of the crystal and the limited angular resolution (FWHM of $\Delta\tau$) of the LEED instrument. The mosaic spread, i.e., the angular distribution of the orientation of individual grains around the averaged [001] direction, has approximately radial symmetry and can be described by its FWHM, $\Delta\Theta$ here. Accounting for both contributions and approximating them with two Gaussian functions, the FWHM at the minima (in phase conditions) of Fig. 1 are given by $\Delta k_{\|} = ck_z$, with $c^2 = (2\Delta\Theta)^2 + \Delta\tau^2$. From this we estimate a FWHM of the mosaic spread $\Delta\Theta = 0.08°$. It is the mosaic spread of the sample that causes the minimal FWHM of the beam profiles to be larger than the nominal instrumental resolution, and thus the *effective* transfer width W ($W = 2\pi/\Delta k_{\|}$) is only 400 Å ($E = 100$ eV), which is far below the nominal instrumental value of 1200 Å.

PHASE DIAGRAM

The section of the phase diagram relevant to the present investigation is shown in Fig. 2. The phase diagram was determined by measurements of intensity versus temperature (I-T) curves at various constant coverages using the temperatures of the respective points of inflection as transition temperatures.[16] Coverages were calibrated from the ratio of Auger peaks at 151 and 272 eV of S and Ru, respectively, assuming perfect order at the maximal transition temperatures of the $p(2\times2)$, $(\sqrt{3}\times\sqrt{3})R30°$, and $c(2\times4)$ structures with corresponding coverages of 0.25, 0.33, and 0.50. A hard sphere model of the $p(2\times2)$ and $(\sqrt{3}\times\sqrt{3})R30°$ superstructures together with the surface Brillouin zone and the diffraction patterns is given in Fig. 3. As seen from Fig. 2, $p(2\times2)$-ordered islands are formed at coverages below $\theta = 0.22$ (phase A) followed by a homogeneous $p(2\times2)$ phase (B) with a maximal critical temperature T_c of 449.0 ± 1 K. With increasing coverages, and at temperatures below 350 K, the coexistence of large $p(2\times2)$ and $(\sqrt{3}\times\sqrt{3})R30°$ ordered islands is observed, which ends in a homogeneous $(\sqrt{3}\times\sqrt{3})R30°$ phase (D) with a maximal T_c of 438.0±1 K. Atoms added to the $(\sqrt{3}\times\sqrt{3})R30°$ phase order as superheavy domain walls in a striped configuration (phase E), whereas they do not order at high enough temperatures close to $\theta = 0.33$ (shaded area in Fig. 2). They are still detectable by broadening of superstructure beam profiles compared to the pure $(\sqrt{3}\times\sqrt{3})R30°$ phase. A characteristic narrowing of profile width as a function of temperature at a constant coverage around 0.35 is interpreted as an order-disorder phase transition of the domain wall phase. Scanning tun-

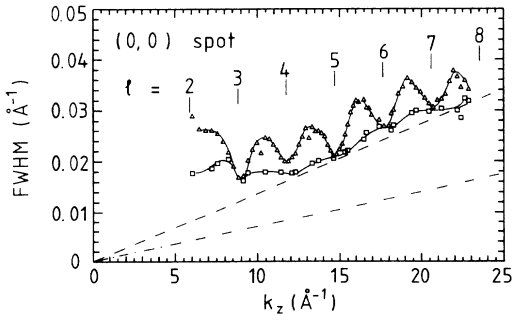

FIG. 1. FWHM of the (0,0) spot versus momentum transfer perpendicular to the surface k_z for two almost perpendicular scan directions [at constant azimuthal angles of 15° (△) and 115° (□) with respect to $\overline{\Gamma M}$]. Dash-dotted line, contribution to the FWHM due to the instrumental resolution alone; dashed line, contribution to the FWHM due instrumental resolution *and* mosaic spread of the sample. In-phase conditions are numbered by the Bragg index ℓ.

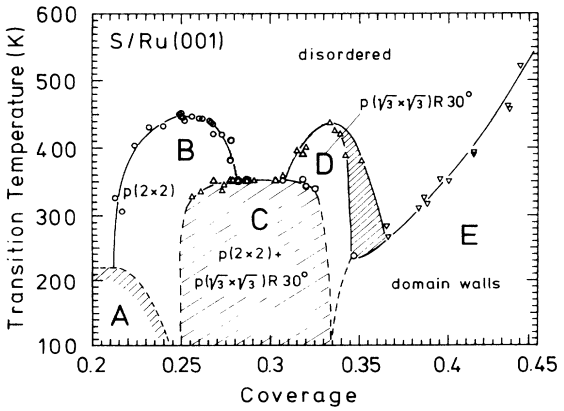

FIG. 2. Phase diagram of S/Ru(001) for coverages Θ between 0.20 and 0.45. Phase A consists of $p(2\times2)$ ordered islands coexisting with a lattice gas. In the hatched area above $\Theta = 0.33$ a $(\sqrt{3}\times\sqrt{3})R30°$ phase with disordered superheavy domain walls is formed.

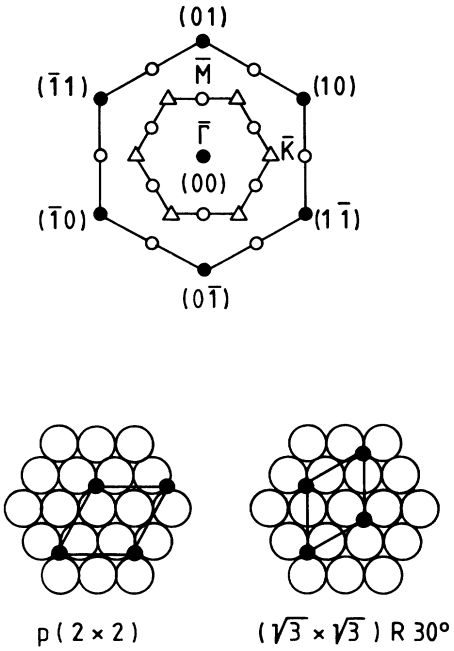

FIG. 3. Surface Brillouin zone with $p(2\times2)$ (○) and $(\sqrt{3}\times\sqrt{3})R30°$ (△) LEED patterns (top) and hard sphere models of the $p(2\times2)$ and $(\sqrt{3}\times\sqrt{3})R30°$ structures.

neling microscopy (STM) investigations show that only one specific adsorption site of threefold coordination is occupied up to coverages 0.33,[18] which is in agreement with a recent LEED-IV analysis.[19] Population of the second threefold adsorption site occurs in phase E. This can be deduced by symmetry arguments from LEED and directly observed by STM.[16,20] Further details of the phase diagram are given in Ref. 16.

In order to avoid Fisher renormalization[21] quantitative evaluations of the critical behavior of the $p(2\times2)$ and $(\sqrt{3}\times\sqrt{3})R30°$ order-disorder phase transitions were only carried out at the respective maxima in the phase diagram.

STRUCTURE FACTOR AND DATA EVALUATION

We parametrized our data using the following form of the structure factor[22,23] from which the exponents β, γ, ν, and η can be extracted:

$$S(\mathbf{k}_\parallel,t) = m^2(t)\delta(\mathbf{k}_\parallel) * \tau(\mathbf{k}_\parallel) + \frac{\chi_0}{(1+\pi^{-2}\xi_x^2k_x^2+\pi^{-2}\xi_y^2k_y^2)^{1-\eta/2}} * \tau(\mathbf{k}_\parallel) + bg(\mathbf{k}_\parallel), \quad (1)$$

with $\mathbf{k}_\parallel = (\mathbf{q}-\mathbf{g})_\parallel$, $\mathbf{q}_\parallel$ the scattering vector, $\mathbf{g}_\parallel$ a reciprocal lattice vector of the superstructure under consideration, and the reduced temperature $t = (T-T_c)/T_c$. The first term contains the order parameter m and stems from the contribution of the long range order that vanishes at T_c as $m^2 \sim |t|^{2\beta}$. The second term describes the correlation function of short range fluctuations (critical scattering) with the correlation length and the susceptibility diverging as $\xi = \xi_0^\pm |t|^{-\nu}$ and $\chi_0 = C_\pm |t|^{-\gamma}$, respectively. The factor of π^{-1} was introduced in Eq. (1) to achieve $\xi = 2\pi\ (\mathrm{FWHM})^{-1}$ where FWHM is the full width at half maximum of the deconvoluted profiles.[24] This definition is useful for the discussion of finite-size effects (see below). The last term denotes a linear background which was also fitted. This structure factor is not exact for the models under consideration, but has proper scaling form for small $\xi q_\parallel$ and small t. The convolution with the instrumental profile $\tau(\mathbf{k}_\parallel)$ is crucial and has to be carried out in two dimensions even for one-dimensional cuts of the beam profile. For reasons of numerical stability, fits to the experimental profiles were carried out instead of direct deconvolutions. For the instrument function we took an experimental profile of minimal half-width measured 20 K below T_c.[7]

For the integrated intensity I_{int} of a superstructure spot, i.e., the intensity measured with the low-resolution Faraday-cup instrument with a small transfer width W compared to the correlation length ξ, the decrease with temperature at a continuous phase transition is given by the exponent α of the specific heat as[25]

$$I_{\mathrm{int}}(t) = \int_{|\mathbf{k}_\parallel|\le k_{\max}} \mathrm{d}^2\mathbf{k}_\parallel\ I(\mathbf{k}_\parallel,t) = A_0 - A_1 t \mp B_\pm |t|^{1-\alpha} + \cdots, \quad (2)$$

where the integration radius $k_{\max}$ is related to W by $k_{\max} = \pi/W$. A_0 and A_1 are positive constants, and the amplitudes B_+ and B_- and the exponents α_+ and α_- refer to situations with $t > 0$ and $t < 0$, respectively. This form of I_{int} is only valid for small t as long as $\xi \gg W$. Further away from the phase transition a crossover to Eq. (1) occurs.[26]

PROFILE EVOLUTION OF SUPERSTRUCTURE SPOTS AND THE DETERMINATION OF T_C

The following description of the results concentrates on the $p(2\times2)$ structure because the principal behavior of the $p(2\times2)$ and $(\sqrt{3}\times\sqrt{3})R30°$ phase transitions is very similar.

Before we turn to the actual analysis of the phase transitions, we survey the evolution of the superstructure profiles as a function of temperature. For this purpose, Fig. 4 shows the inverse FWHM of the first order superstructure spot profiles (undeconvoluted) for two perpendicular scan directions ($\overline{\Gamma M}$ and $\overline{MK}$) versus temperature. (For the determination of T_c, see below.) Remarkably, three temperature regions with different trends of $(\mathrm{FWHM})^{-1}$ are observed for both scan directions. In the first region $T \le (T_c - 15\ \mathrm{K})$, the $(\mathrm{FWHM})^{-1}$ is constant, demonstrating that the temperature increase leads only to uncorrelated point defects. The values of $2\pi(\mathrm{FWHM})^{-1}$, which can be regarded as a measure for the average domain

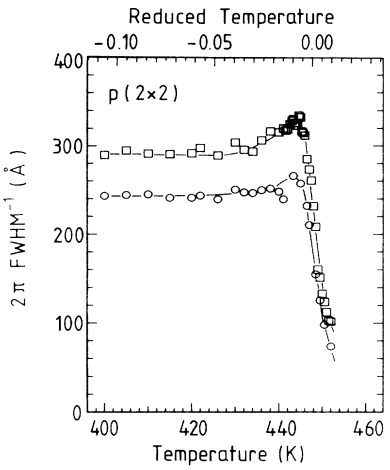

FIG. 4. Inverse FWHM (average domain size) of a $p(2\times2)$ first order superstructure spot along the $\overline{\Gamma M}$ (□) and $\overline{MK}$ (○) directions as a function of temperature.

size, are ~290 and ~240 Å. Both values are below the effective transfer width of the instrument of 400 Å, but close to the average terrace width. Therefore, it seems that the $p(2\times2)$ correlations end at the monatomic steps. This model is proved in detail by the experiments on the higher step density surfaces reported below. The above values do not exactly agree with the average step distance of 275 Å since none of the scan directions was aligned to the step directions and since undeconvoluted profiles were considered. In the second region, for $(T_c - 15\ \text{K}) \leq T \leq (T_c - 5\ \text{K})$, the profiles show a small narrowing (<10% of their FWHM). It is reversible and must be due to spontaneous disappearance of antiphase domains as the temperature is raised because of partial depinning of adsorbate domains from step edges at temperatures close to the phase transition. This is the second indication for a considerable interaction of the sulfur layers with the steps (see below). The disappearance of antiphase boundaries indicates an increased mobility of the sulfur atoms in a small temperature interval below T_c. This might be an indirect hint of the presence of critical fluctuations below T_c, although the intensity of those critical fluctuations below T_c is very small in 2D phase transitions,[27] so that this contribution to the spot profiles could not be detected in the profile analysis (see below). In the third temperature region $T \geq (T_c - 5\ \text{K})$, the $(\text{FWHM})^{-1}$ decreases rapidly, demonstrating the thermal excitation of antiphase boundaries with the onset of critical fluctuations when the phase transition is passed. In fact, the broadening of the FWHM starts already at ~5 K *below* T_c. This is interpreted as a consequence of the rounding of the transition by finite-size effects, which will be analyzed further below. No peak shift is observed, indicating a transition to a disordered lattice gas.

The value of T_c was determined from the optimization of power-law behavior of the data both below and above T_c (see below) as well as from the points of inflection in I-T curves of peak intensities and integrated intensities. All values coincided within ±0.5 K. The use of the inflection points of peak intensity curves for the determination of T_c (Ref. 25) was still possible with reasonable accuracy for the nominally flat surface, since there the transfer width of 400 Å is not far beyond the maximal correlation lengths (see below). However, this is no longer true for the vicinal surfaces with much smaller maximal correlation lengths (see below).

CRITICAL EXPONENTS

In order to determine the exponent β of the order parameter, data of peak intensities, i.e., the intensities of the spot maxima, are plotted versus temperature and reduced temperature in Fig. 5 after dividing out the Debye-Waller factor. It was estimated from extrapolations of low temperature data to $T = 0$ K.[7] We obtained an effective Debye temperature of 540 K using the mass of a single Ru atom. Approximate power-law behavior [according to the first term in Eq. (1)] can be observed within $0.01 \leq |t| \leq 0.1$ whereas for smaller $|t|$ deviations due to the finite-size effects can be seen. The

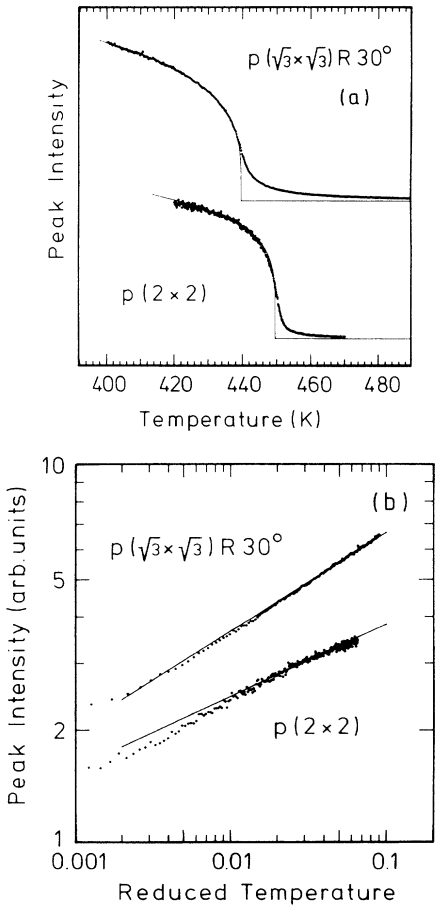

FIG. 5. (a) Peak intensities versus temperature for the order-disorder phase transitions of the $p(2\times2)$ and the $(\sqrt{3}\times\sqrt{3})R30°$ structure after division by the Debye-Waller factor. Solid lines: fits to a power law $m^2 \sim |t|^{2\beta}$. Left ends of horizontal lines mark T_c. (b) Log-log plots of peak intensities versus reduced temperature $t = (T - T_c)/T_c$ below T_c. Lines: average slope of data for $0.01 \leq |t| \leq 0.1$.

effective exponents β obtained as averages over 7 – 8 of these plots are $\beta = 0.11 \pm 0.02$ for the $p(2\times2)$ and $\beta = 0.14 \pm 0.03$ for the $(\sqrt{3}\times\sqrt{3})R30°$ phase transitions. These values are ~30% larger than those expected for the three- and four-state Potts universality classes, respectively, and seem to be influenced by corrections to scaling. A separation of the corrections, however, is not possible here because of the small range in $|t|$. Especially, in the four-state Potts class logarithmic corrections for the order parameter are expected.[28] The inclusion of this type of correction, however, did not improve the quality of the fits for the accessible range of t. Significant contributions from critical scattering in the considered interval of $t \leq -0.01$, on the other hand, can be excluded by profile analysis. This result is in agreement with theoretical estimates of very large ratios of the amplitudes $C_\pm$ above and below T_c of 2D phase transitions[27] and MCS for the $p(2\times2)$ and $(\sqrt{3}\times\sqrt{3})R30°$ phase transitions which yielded $C_+/C_- \simeq 40$.[29]

For an evaluation of the exponents γ, ν, and η only the temperature range above T_c was used. Fits to the experimental profiles according to Eq. (1) were carried out either with the full expression allowing $\xi_x \neq \xi_y$ and $\eta \geq 0$, using a 2D Fourier transformation for the convolution with the instrument function or, for better numerical stability and smaller computing times, under the additional restrictions $\xi_x = \xi_y$ and $\eta = 0$ using the algorithm already described in Ref. 7. (For $\eta = 0$ the Ornstein-Zernike approximation[22] is fitted.) A set of typical fits for the $p(2\times2)$ structure is displayed in Fig. 6. Values of ξ and χ_0, fitted with $\xi_x = \xi_y$ and $\eta = 0$, are plotted versus reduced temperatures in Fig. 7 for the $p(2\times2)$ phase transition. A similar plot for the $(\sqrt{3}\times\sqrt{3})R30°$ structure is shown in Fig. 8. For both phase transitions

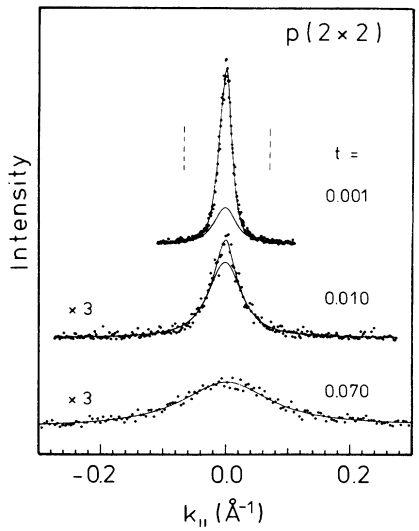

FIG. 6. Spot profiles of a $p(2\times2)$ first order superstructure spot along the $\overline{\Gamma M}$ direction slightly above T_c, as indicated. The lines mark fits to the experimental data points according to Eq. (1). Lower line: contribution to the profile of the critical scattering alone (Lorentzian shape, η fixed to 0). The vertical dashed lines indicate the integration range of the low-resolution Faraday-cup instrument.

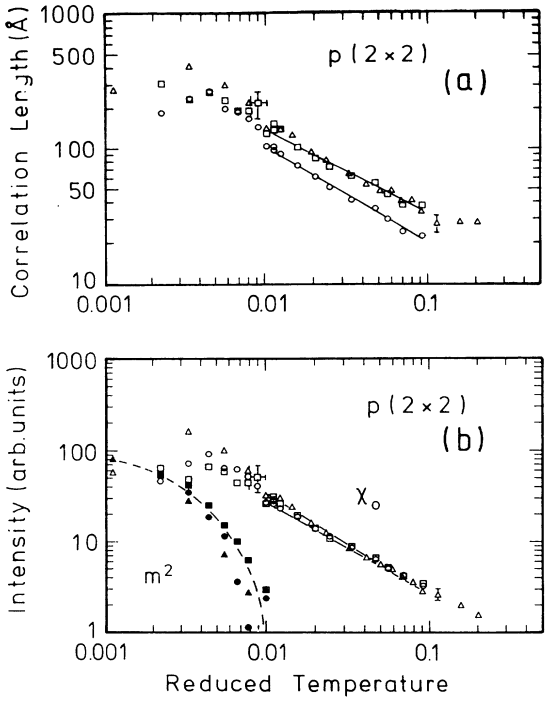

FIG. 7. Log-log plots of (a) fitted correlation lengths ξ and (b) susceptibilities χ_0 and m^2 versus reduced temperature above T_c for the $p(2\times2)$ structure. Different symbols mark different cuts through the spots: □, $\overline{\Gamma M}$ direction; ○, $\overline{MK}$ direction; △, 15° with respect to $\overline{\Gamma M}$. Lines are maximal and minimal slopes compatible with single data sets.

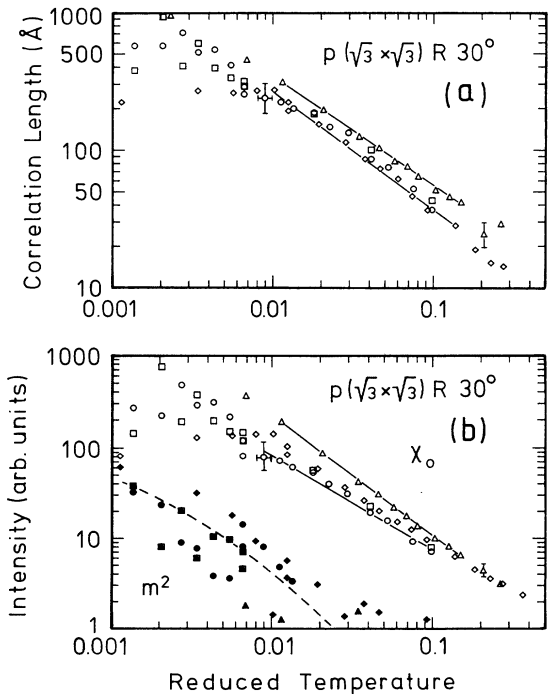

FIG. 8. Log-log plots of (a) fitted correlation lengths ξ and (b) susceptibilities χ_0 and m^2 versus reduced temperature above T_c for the $(\sqrt{3}\times\sqrt{3})R30°$ structure. Same symbols as in Fig. 7 are used: □, $\overline{\Gamma M}$-direction; ○ and ◇, $\overline{MK}$ direction; △, 15° with respect to $\overline{\Gamma M}$.

both types of fits yielded the same exponents, only the amplitudes differed by 15 – 20 % for ξ and by up to 50% for χ_0. As can be seen from Figs. 7 and 8, the above mentioned changes in ξ and χ_0 due to the two different fit procedures would be still within the overall uncertainties of the determination of the fit parameters, which justifies to use mainly the faster fit procedure with $\eta = 0$.

Figures 7 and 8 clearly reveal the presence of finite-size effects for reduced temperatures below $t \leq 0.01$ for two reasons. First, the divergence of the correlation length and the susceptibility levels off at $t \approx 0.01$. Second, for data below $t = 0.01$ an inclusion of the first term in Eq. (1) gave better fits to the data than a fit to the second term alone, and thus values of $m^2 > 0$ are observed. This must be due to finite size effects, since the long range order, which is responsible for the m^2 term below T_c, vanishes at the phase transition by definition. Thus values of $m^2 > 0$, for $T \geq T_c$, are *not* indicative for a persisting long range order but for the influence of finite-size effects on the critical fluctuations. (For $T \geq T_c$ the parameter m should not therefore be called an order parameter.) Values $m^2 > 0$ above T_c indicate that the correlation functions differ from the ideal ones because the longer correlations are suppressed by the finite size effects. Therefore, they do not fall off exponentially on all length scales, which would give exclusively the second (Lorentzian) term, but result in spot profiles which can be better approximated by a sum of the first two terms in Eq. (1). Consequently, the values for the correlation lengths fitted in the finite-size-rounded temperature regime should not be interpreted as exponential decay lengths of correlations. Instead, it is more appropriate to interpret the inverse FWHM of the fitted Lorentzian profile as the average size of temporarily $p(2\times2)$ ordered domains. In the parametrization used for ξ (see above) it is thus possible to compare the upper limits of ξ with those values deduced for the average terrace width. Maximal values of ξ are ~200 Å [$p(2\times2)$] and ~300 Å [$(\sqrt{3}\times\sqrt{3})R30°$], and agree well with the average terrace width of ~275 Å. Thus we conclude that the critical fluctuations end at the steps (as the static order below T_c does) and that the steps are mainly responsible for the finite-size rounding of the transitions. This interpretation of the finite-size-affected profile form is corroborated by the additional experiments on the vicinal surfaces. The slightly larger values of the maximal correlation length obtained for the $(\sqrt{3}\times\sqrt{3})R30°$ phase transition are likely to be due to an increased average terrace width that results from a partial change of the surface morphology at higher S coverages, which could be observed in detail on the vicinal surfaces.[30] A totally different interpretation would be that the observed profiles consist of an incoherent superposition of intensities scattered from long range ordered and from short range ordered regions, but this would imply a local variation of T_c (due to a local variation of coverage) or a variation of T. Both possibilities can be excluded, since extreme care was taken to prepare homogeneous coverages (see above). In addition, the temperature averaging of the experiment (0.4 K) was smaller by approximately one order of magnitude than the width of the finite-size-affected temperature region.

The influence of the finite-size effects vanishes further away from the phase transition when the correlation length falls far below the average step distance. As a consequence, only the data for $t \geq 0.01$ can be used for the determination of exponents from power-law fits. Similar to the peak intensities below T_c scaling, i.e., power-law behavior, for χ_0 and ξ was found again in the range $0.01 \leq |t| \leq 0.1$ with exponents $\gamma = 1.04 \pm 0.08$ and $\nu = 0.66 \pm 0.06$ for the $p(2\times2)$ transition. The corresponding values for the $(\sqrt{3}\times\sqrt{3})R30°$ transition are $\gamma = 1.18 \pm 0.14$ and $\nu = 0.81 \pm 0.09$. Most of the uncertainties are due to corresponding uncertainties in T_c, but can also be partly caused by small variations in coverages during the experimental runs (see above).

Figures 7 and 8 also show that ξ is not isotropic for both phase transitions with a maximal ratio of amplitudes in different scan directions of 2 for the $p(2\times2)$ and 1.7 for the $(\sqrt{3}\times\sqrt{3})R30°$ structure. This could be an effect of the anisotropy introduced by the steps. On the other hand, spot profiles in general only have the symmetry of the respective points on the Brillouin zone edge and need not be isotropic.[29] As this anisotropy is not affected by the step density, the latter possibility seems to be more relevant.

For the $p(2\times2)$ structure the quality of the data was sufficient to include the exponent η as an additional fit parameter. Values of $\eta > 0$ lead to softer profile wings and improve the quality of the fits slightly for values of $\xi k_{\|} \geq 2$ with respect to fits with $\eta = 0$. Two fits with $\eta = 0$ and $\eta > 0$ are compared in Fig. 9(a). The difference between the two fits is small since the influence of η on the profile wings can be also partially obtained for the fits with $\eta = 0$ by larger values of the correlation length in combination with an increase of the linear background. The fitted values of η are given as a function of temperature in Fig. 9(b). The exponent η turns out to be temperature independent with an average value of $\eta = 0.27 \pm 0.2$ for the p(2×2) transition. The large error bar is mainly caused by the uncertainties in background determination which strongly influence the value of η. The results for all determined critical exponents are given in Table I.

In order to test whether the integrated intensities (I_{int}) measured with the low-resolution Faraday-cup instrument scale too, we analyzed them according to Eq. (2). The data were taken at an energy of 57 eV and the transfer width W was approximately 50 Å. For the measured first order $p(2\times2)$ and $(\sqrt{3}\times\sqrt{3})R30°$ superstructure spots this corresponds to an integration area of 0.24% and 0.23% of the surface Brillouin zone, respectively (see also Fig. 6). These intensities I_{int}, are plotted versus temperature in Fig. 10(a) and versus reduced temperature on log-log scale in Fig. 10(b). Power-law fits to the data with the exponents α fixed to the theoretical values of the four-state- ($\alpha = 2/3$) and three-state Potts model ($\alpha = 1/3$), respectively, and A_1 fixed to zero are shown as lines. The value T_c was determined from the inflection point of the data.[25]

It is obvious from Fig. 10(b) that the data for $T \leq T_c$ follow approximately a power law for $0.01 \leq |t| \leq 0.10$

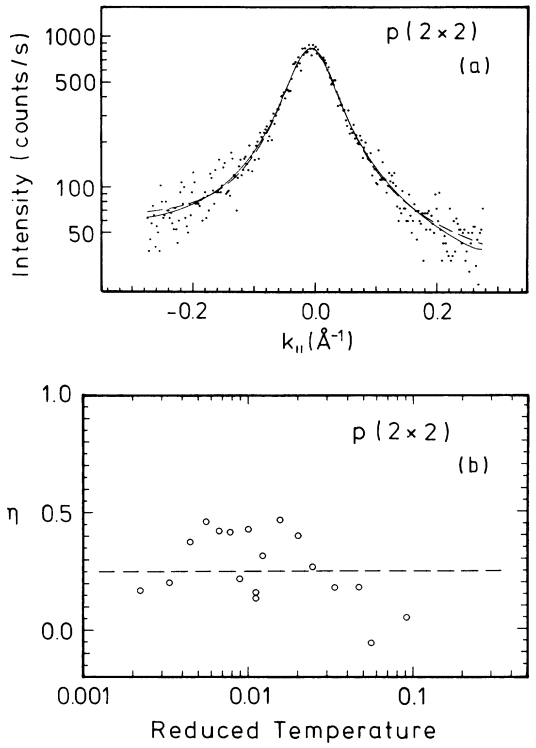

FIG. 9. (a) Spot profile of the $p(2\times2)$ first order superstructure spot ($\overline{MK}$ direction). Solid line, fit with η fixed to 0; dashed line, fit with $\eta = 0.31$ according to Eq. (1). (b) Fitted values of the exponent η versus reduced temperature above T_c. Dashed line, theoretical value $\eta = 0.25$ of the four-state Potts model.

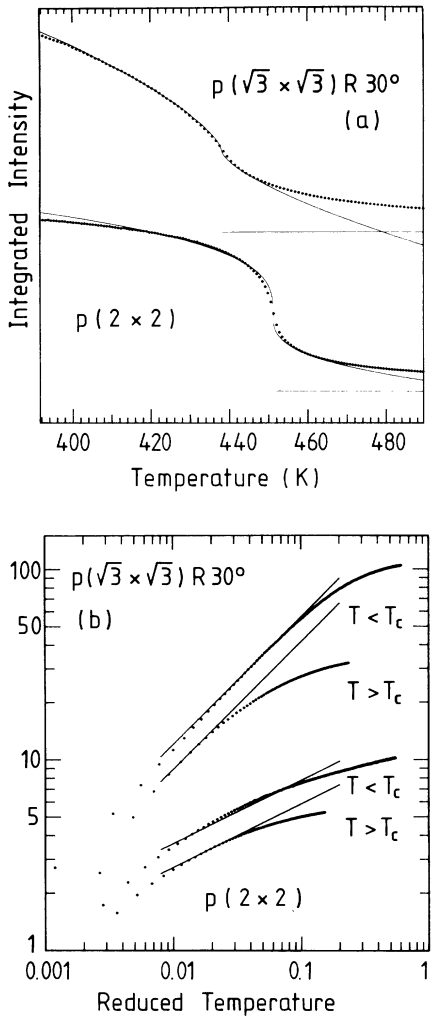

FIG. 10. (a) Integrated intensities ($I_{\rm int}$), measured with the low-resolution Faraday-cup instrument, versus temperature for the $p(2\times2)$ and the $(\sqrt{3}\times\sqrt{3})R30°$ structures after division by the Debye-Waller factor. Solid line, fit to a power law $A_0 + B_\pm|t|^{1-\alpha}$. (b) Log-log plots of $|I_{\rm int}|t| - I_{\rm int}(0)|$ versus absolute reduced temperature below and above T_c. Lines, same power-law fit to the data as in (a).

for both phase transitions, whereas this range is much smaller for the data at $T > T_c$. The ratio of the amplitudes B_-/B_+ is approximately 1.3 for both the $p(2\times2)$ and $(\sqrt{3}\times\sqrt{3})R30°$ phase transitions. We interpret the deviations from power-law behavior to be partly due to a violation of the integration condition $\xi k_{\rm max} \gg 1$ and partly due to the presence of corrections in the temperature range considered. The deviation of the ratio of B_-/B_+ from the theoretical value of 1 for the Potts models[31] might be an effect of these corrections to scaling. One reason for the better power-law behavior for $T \leq T_c$ may be that for T *below* T_c the intensity is composed of a dominant contribution of the long range order [with a temperature independent profile shape with a FWHM$\ll 2\pi/W$; cf. Eq. (2)] and the critical scattering, whereas *above* T_c only critical scattering contributes. In comparison to the data measured earlier for the $p(2\times2)$ phase transition of oxygen on the same surface[7] the deviations from power-law behavior are more significant here, which we attribute to the smaller integration radius used here because of experimental reasons.[32] These results show that the exponent α can in principle be determined by this method. However, the results depend crucially on the experimental conditions and their exact definition so that they are less reliable than the determination of other critical exponents.

TABLE I. Comparison of experimental and theoretical critical exponents (see Ref. 31).

	$p(2\times2)$	Four-state Potts	$(\sqrt{3}\times\sqrt{3})R30°$	Three-state Potts
β	0.11 ± 0.02	0.083	0.14 ± 0.03	0.11
γ	1.04 ± 0.08	1.17	1.18 ± 0.14	1.44
ν	0.66 ± 0.06	0.67	0.81 ± 0.09	0.83
η	0.27 ± 0.2	0.25		0.27

INTERACTIONS WITH STEPS AND FINITE-SIZE EFFECTS

To obtain further information about the interaction of the superstructures with steps and to study the influence

of the steps on the phase transitions explicitly, we have performed additional experiments on the two vicinal surfaces with average terrace widths Λ of 33 Å and 85 Å, respectively. The quantitative experiments concentrated on the $p(2\times2)$ superstructure since an analogous situation is observed for the $(\sqrt{3}\times\sqrt{3})R30°$ superstructure. The preparation of sulfur layers of defined coverages by thermal desorption is difficult on these vicinal surfaces, as heating to temperatures above 700 K causes changes of the surface morphology via step doubling and facetting.[30] These complications were avoided by dosing H_2S at 500 K (Ref. 33) and limiting the annealing cycles to temperatures below 500 K. The step morphology was controlled by the (0,0)-spot profile.[9] In the phase diagram, up to coverages of 0.5, only small changes in the positions of the phase boundaries (less than 5%) were observed on the stepped surface with 85 Å wide terraces with respect to the nominally flat surface. Optimal coverages for the $p(2\times2)$ and $(\sqrt{3}\times\sqrt{3})R30°$ phase transitions were obtained by maximizing the inflection points of the I-T curves (see above).

We start with the examination of the position of the $p(2\times2)$ superstructure domains relative to the steps. For this purpose profiles of superstructure spots were measured on the 33 Å stepped surface at different energies. Figure 11 displays a set of such profiles for first order superstructure spots in the direction perpendicular to the steps. For those spots where the scattering vector $\mathbf{k}_{\|}$ has a zero or integer component parallel to the step edges, for the $(\frac{1}{2},0)$ spot, e.g., the profile is composed out of two peaks: a broad peak with a FWHM $= 2\pi/\Lambda$ and a sharp peak with a FWHM of the order of the instrumental resolution. As can be seen from Fig. 11, the relative contributions of the two peaks vary with energy.[34] For spots with a non-integer component of $\mathbf{k}_{\|}$ parallel to the step edges, the profile consists systematically only of the broad peak [see, for instance, the $(1,\frac{1}{2})$ spot in Fig. 11]. In the direction parallel to the steps, all profiles have FWHM close to the instrumental resolution.

The observed profiles are only compatible with a model of $p(2\times2)$ domains pinned at the positions of the step edges on each terrace and with essentially no interaction between S atoms on different terraces so that order is limited to one terrace. The pinning must be due to adsorption energies higher at specific adsorption sites at steps compared to all other sites. Under this condition, the scattered intensity can be separated into two parts. One stems from the interference between $p(2\times2)$ domains on different terraces, the other from the interference within individual terraces. Details of this model are given by Kleban.[35] The interface scattering provides the sharp peak, which is a consequence of the spatial correlations of the sulfur domains induced by the periodic arrangement of the steps. This contribution is absent for spots with a noninteger component of $\mathbf{k}_{\|}$ in the direction parallel to the step edges, for the $(1,\frac{1}{2})$ spot, e.g., since no correlation of the $p(2\times2)$ domains parallel to the steps can be induced by the pinning. The interface scattering causes the broad peak with a FWHM corresponding to the inverse terrace width. This contribution is present for all spots. It would be the only one, if the positioning of the $p(2\times2)$ domains were fully random; such a situation is found for the p(2×2) domains of oxygen on this surface at coverages below 0.18.[9] Qualitatively identical spot profiles are observed for the 85 Å surface, although the two components cannot be separated as easily due to the increased terrace width.

We now turn to the influence of the steps on the critical behavior at the phase transitions which we studied on the 85 Å surface in detail and compared the results to those of the nominally flat surface (Λ = 275 Å). In order to demonstrate the stronger finite-size rounding, peak intensities versus temperature are shown for both surfaces in Fig. 12. The maximal slope of the curve of the 85 Å surface is reduced by approximately a factor of 4 compared to the curve for the 275 Å surface, which indi-

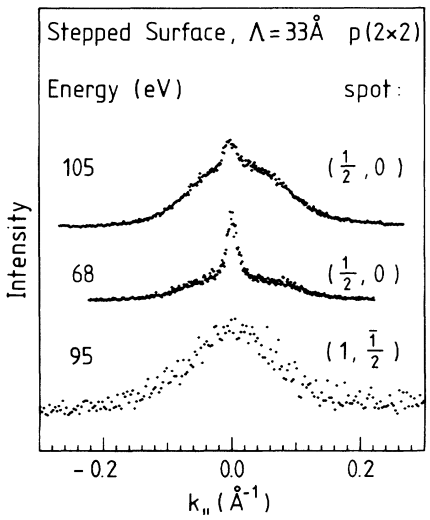

FIG. 11. Profiles of first order $p(2\times2)$ superstructure spots measured on the vicinal surface (terrace width Λ = 33 Å) in the direction perpendicular to the steps ($\overline{\Gamma M}$), T = 100 K.

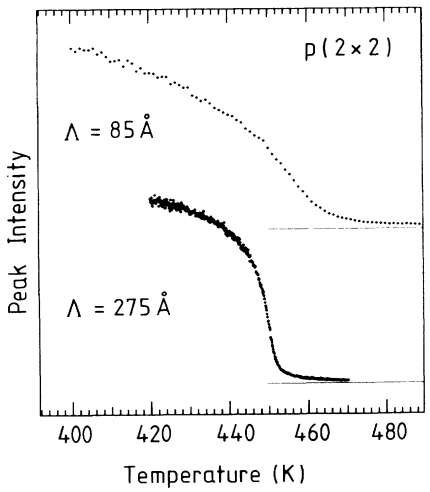

FIG. 12. Comparison of peak intensities versus temperature for the $p(2\times2)$ phase transitions on the nominally flat surface with terrace width Λ_1 = 275 Å and the vicinal surface with Λ_2 = 85 Å. Left ends of horizontal lines mark T_c.

cates finite-size rounding over a much larger temperature range. This is expected from theory, as the temperature interval, where the curve of the finite system deviates from the curve of the ideal system as a function of the characteristic system size l scales with $l^{\frac{1}{\nu}}$.[36] Quantitative estimates of the rounded region can be given from profile analyses described below.

The stronger finite-size rounding also influences the determination of T_c, as for this surface T_c deviates from the position of the inflection point of the (peak) intensity curve (in contrast to the 275 Å surface). This can be easily explained since ξ remains small compared to the transfer width of 400 Å, and therefore the condition $k_{\max}\xi \gg 1$ is not fulfilled. Instead T_c was determined from the optimization of power-law dependence both for χ_0 and ξ (see below). T_c determined in this way was found to be consistently 3–5 K higher than the inflection points. The value obtained for T_c is 450±3 K and agrees within error limits with the value determined for the 275 Å surface (449.0 ± 1 K). Although the temperature values may be subject to small additional systematic errors ($\leq$5 K) of different thermocouples we can exclude a significant shift in T_c due to finite-size effects.

In order to study the finite-size effects more quantitatively, we evaluated the profiles of the $(\frac{1}{2},0)$ spot at temperatures above T_c according to Eq. (1), similar to the nominally flat surface. For the instrument function we took a profile which corresponded to the sharp peak of the spot profile. In this analysis the long range order contribution $[m^2\delta(\mathbf{k}_\parallel) * \tau(\mathbf{k}_\parallel)]$ was fitted to the interterrace scattering of the averaged $p(2\times2)$ domains (sharp peak in Fig. 11) and the critical fluctuations $[\chi(\mathbf{k}_\parallel) * \tau(\mathbf{k}_\parallel)]$ are fitted to the intraterrace scattering (broad peak). Figure 13 shows the values obtained for ξ, χ_0, and m^2.

As can be seen from this figure the range, where power-law behavior is observed, is further reduced, but within error limits we obtain the same values for the critical exponents γ and ν ($\gamma = 0.86 \pm 0.1$, $\nu = 0.66 \pm 0.1$) as on the nominally flat surface. A small difference in the slopes is observed for the χ_0 data, which, however, is still within the error limits. In fact, the correlation lengths in both scan directions, perpendicular and parallel to the steps, are limited by the average terrace width. These findings demonstrate that no crossover to a quasi-one-dimensional system occurs when ξ approaches the average terrace size Λ. The finite-size rounding observed for ξ is also in quantitative agreement with finite-size scaling theory,[37] which requires that $\xi \sim l\,Q_\xi(x)$ with $x = l^{1/\nu}t$, where l is the characteristic system size. We took $l = \Lambda/a$, a being the lattice constant. In addition, $\chi_0 \sim l^{\gamma/\nu}Q_\chi(x)$ is predicted by theory. Both functions $Q_\xi(x)$ and $Q_\chi(x)$ depend only on the boundary conditions, but should be universal as long as these do not change.[37] Plots ξ/l versus x for the 85 Å and the nominally flat surface gave reasonable agreement and similar leveling off for ξ was obtained for $\xi/\Lambda \to 1$. While the second proportionality $[\chi_0 \sim l^{\gamma/\nu}Q_\chi(x)]$ cannot be tested directly in the experiment, because of experimental difficulties in comparing absolute intensities measured on different crystals, the ratio m^2/χ_0 at constant x can test whether $Q_\chi(x)$ scales. Within rather large error bars

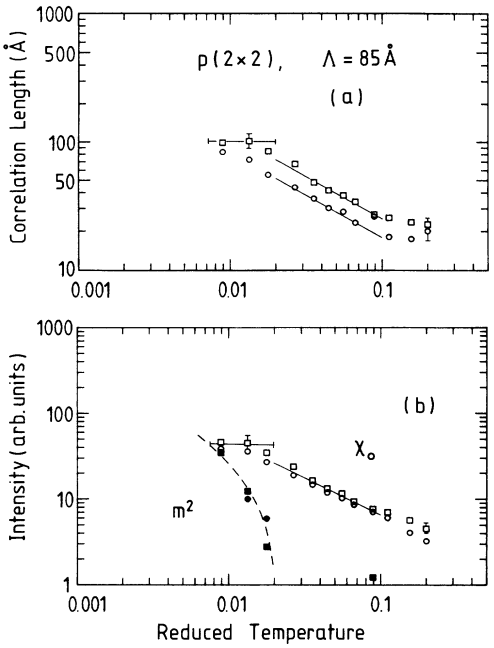

FIG. 13. Log-log plots of (a) fitted correlation lengths ξ and (b) susceptibilities χ_0 and m^2 versus reduced temperature above T_c for the $p(2\times2)$ structure on the vicinal surface with Λ_2 =85 Å wide terraces.

the same ratios were found, indeed, on the two surfaces tested for an x range between 1 and 10. The scatter of data, however, does not seem to contain any systematics, so that semiquantitative agreement with theory can be concluded.

Remarkably, for ξ we find the same amplitude ratios for the different scan directions for both surfaces. This demonstrates again that the anisotropy of ξ is not due to the influence of steps. This analysis reveals that the main influence of steps in this system is to limit the correlation length to one terrace. The resulting finite-size effects agree with the expectations from finite-size scaling theory.

DISCUSSION

Although the effective exponents determined in our study for the $p(2\times2)$ and the $(\sqrt{3}\times\sqrt{3})R30°$ order-disorder phase transitions of S on Ru(001) do not match exactly those which are expected theoretically for the four-state Potts and the three-state Potts universality classes,[31] they are closest to these classes. Deviations from the exact values due to corrections to scaling can be expected for the accessible temperature range $0.01 \leq |t| \leq 0.1$, where the data can be described by power-law fits. As these effective exponents still obey scaling laws (see below), it seems to be fully justified to claim that these phase transitions are continuous.

This assignment is in agreement with the first of the Landau rules,[1] if adsorption of sulfur takes place on high symmetry sites (top or threefold coordinated hollow sites), and the same type of site is occupied in both

the ordered and the disordered phases. Whereas the geometry of the disordered phase has not yet been determined, adsorption solely on the threefold coordinated hcp site (hollow site without substrate atom below S in the second substrate layer) has indeed been found for both phases.[19] From our findings of continuous phase transitions this adsorption site should also be maintained in the disordered phase. It is an interesting and still not answered question how strictly this rule must be fulfilled without changing the character of the phase transitions. Occupation of additional sites may be one reason why the order-disorder transition of O/Ni(111) does *not* show the expected four-state Potts behavior.[38,39]

A continuous phase transition in the four-state Potts universality class has also been found for the order-disorder transition of the $p(2\times2)$ structure of oxygen on the same surface[7] so that both results can be easily compared. Interestingly, the interactions with steps in these two systems are very different, although the critical behavior of the $p(2\times2)$ structures of S and O on Ru(001) (Ref. 7) is very similar. For O the lateral interactions between the atoms are sufficiently strong to extend $p(2\times2)$ correlations across steps,[30] whereas for S these interactions are weaker so that correlations end at steps. This difference in interaction strength is expressed roughly in the difference of critical temperatures (750 K and 450 K, respectively). It is also found in the adsorbate induced relaxations of the substrate atoms of the first two substrate layers. For $p(2\times2)$ ordered oxygen these are approximately twice as large as for the same structure of S. As the lateral interactions are mediated by the substrate, these relaxations should also reflect the strength and the effective range of interactions.

As a consequence of the different strength of interaction in these systems, the influence of the steps on the phase transitions is totally different. For O a crossover to Ising behavior occurs due to the reduced symmetry[8] of the whole system containing many steps within the correlation length. In contrast, for sulfur pronounced finite-size rounding occurs. This behavior is more similar to the one observed for the $p(2\times1)$order-disorder phase transition of O at half monolayer coverage.[40] These pronounced finite-size effects were limiting for the observation of scaling for S/Ru resulting in clearly visible corrections to scaling. On the other hand, they allowed a closer investigation of these effects.

Deviations especially of the exponents β and γ from the theoretical values indicate that corrections to scaling are in fact present for the $p(2\times2)$ and $(\sqrt{3}\times\sqrt{3})R30°$ phase transitions of S/Ru(001). Whereas the experimental values for the exponents β and γ come out larger by $\sim$30% and smaller by $\sim$20%, respectively, compared to the theoretical values (see Table I), the agreement of the theoretical and the experimentally determined values of ν is very good (within a few percent). Interestingly, the deviations for β and γ compensate each other so that the scaling law $\nu=\frac{1}{2}\gamma+\beta$ (Ref. 22) is still fulfilled within experimental errors for both phase transitions.

It is instructive to compare the exponents obtained here with those of the $p(2\times2)$ order-disorder phase transition of oxygen on the same surface[7] and those found in a MCS of the $p(2\times2)$ and $(\sqrt{3}\times\sqrt{3})R30°$ superstructures on triangular nets by Bartelt, Einstein, and Roelofs.[29] Smaller values for γ and relatively good agreement for ν with respect to Potts values were also observed in these systems. This seems to indicate that similar corrections to the exponents, probably due to the same higher order terms of the Hamiltonians, are present in the experimentally accessible not-finite-size-affected ranges of t in all these systems. This means that neither Monte Carlo simulations nor experimental data have been extended to sufficiently small values of t so that the pure Potts exponents could be observed.

These corrections are probably stronger than in Potts models due to the fact that the Landau-Ginzburg-Wilson Hamiltonians of the $p(2\times2)$ and $(\sqrt{3}\times\sqrt{3})R30°$ phase transitions on a lattice gas are only identical with the respective Potts Hamiltonians in the leading terms. Only in the limit of $\xi\to\infty$ the higher order terms are expected to become negligible so that the same (universal) behavior is obtained.[29] Corrections might also be the reason why the observed ratios of the amplitudes of the specific heat B_-/B_+ are different from 1, the value of the Potts models. The anisotropy of the correlation length observed in our experiments, which again is not present in the Potts models, is most likely due to the influence of the symmetry of the lattice, which differs from that of a Potts system, and reflects the symmetry of the corresponding Bragg point in the surface Brillouin zone. Therefore, isotropic behavior can only be expected very close to the Bragg point, where measurements in our case are strongly influenced by finite size effects. Because of the highly symmetric adsorption site the anisotropy *cannot* be due to simple lattice anisotropy,[29] which in the related Ising-model on a rectangular lattice was found to be a marginal parameter leading to anisotropic scaling of the correlation length with the same exponent ν for different directions.[41] Instead, in the present system the anisotropy could be due to higher order terms in the Hamiltonians which break the degeneracy for the excitation of antiphase boundaries in different directions with respect to the substrate to vanish only in the limit of $\xi\to\infty$.[29] An anisotropy for ξ was also observed in MCS of the $p(2\times2)$ and $(\sqrt{3}\times\sqrt{3})R30°$ phase transitions.[29] In the case of the $p(2\times2)$, a ratio $\xi_{\overline{\Gamma M}}/\xi_{\overline{MK}}\simeq0.85$ was observed for $0.01\le t\le0.1$, whereas we observe $\xi_{\overline{\Gamma M}}/\xi_{\overline{MK}}\simeq2$. This obviously system specific difference is not understood yet.

The exponent η of the $p(2\times2)$ structure was determined here using the common Fisher approximation for the structure factor [see Eq. (1)]. Although this is the simplest parameterization, one should bear in mind that its reliability for the determination of η from profile fits has been questioned in the case of the Ising model.[42] Nevertheless, this analysis of the data seems to be meaningful because the experimentally determined exponent η is not dependent on temperature. Therefore, the $p(2\times2)$ structure factor possesses the scaling behavior of Eq. (1). The value found is in good agreement with the theoretically expected one, but in view of the large scatter of the data this may be accidental. Considering Fisher's scaling law $\eta=2-\gamma/\nu$, values for η of 0.42 and 0.56 are calculated

for the $p(2\times2)$ and $(\sqrt{3}\times\sqrt{3})R30°$ phase transitions, respectively. For the $p(2\times2)$ this value is at the upper limit of the determination of η by the profile fit.

Finally, we note that the difference between experimental and theoretical exponents cannot be due to Fisher renormalization[21] because this would cause a shift to larger values for *all* exponents, e.g., $\gamma' = \gamma/(1-\alpha)$, which we do not observe. A further reason could be that the theoretical models are not fully applicable to the experimental situations since the underlying lattice gas model, i.e., the exclusive population of only one adsorption site in the ordered and in the disordered phases, may be violated by a thermally activated spillover of the S atoms onto less favorable adsorption sites at elevated temperatures. The influence of this effect on critical behavior was demonstrated recently for the order-disorder phase transition of $p(2\times1)$ ordered oxygen by MCS.[43] Such a mechanism, however, would be more likely for the $(\sqrt{3}\times\sqrt{3})R30°$ phase transition since adsorption on the second threefold site starts at coverages above the $(\sqrt{3}\times\sqrt{3})R30°$ phase,[16] but should be less important for the $p(2\times2)$. Since the deviations of experimental from theoretical exponents observed are of the same order for the $p(2\times2)$ and $(\sqrt{3}\times\sqrt{3})R30°$ phase transitions, we conclude that this mechanism is not mainly responsible for the observed deviations.

SUMMARY AND CONCLUSIONS

The order-disorder phase transitions of the $p(2\times2)$ and $(\sqrt{3}\times\sqrt{3})R30°$ superstructures on the Ru(001) surface are both continuous and the effective critical exponents can be determined by a temperature resolved low-energy electron diffraction experiment within a scaling range of one order of magnitude in t. Scaling laws are fulfilled within error bars. The values of the exponents fall close to those of the four- and three-state Potts universality classes, respectively, indicating that the four- and three-state Potts models provide the correct descriptions of the two phase transitions in the limit of diverging ξ. Nevertheless, the deviations between theoretical and experimental exponents, especially for γ, and the significant anisotropy observed for ξ indicate the presence of corrections to scaling. These are likely to be due to higher order terms in the respective Hamiltonians, which play a role in the accessible scaling range $0.01 \leq |t| \leq 0.10$. These higher order terms might be more significant than in pure Potts models due to the lattice-gas character of the systems.

The interaction of sulfur with monoatomic steps limits the correlation length at the phase transition, leading to finite-size effects which scale according to finite-size scaling theory with the average terrace width as the characteristic length. In this system it is thus possible to study the scaling behavior as a function of the system size by use of vicinal surfaces with a well defined step density, in addition to scaling in the temperature domain. For the typical surface qualities, with 300 Å wide terraces, finite-size effects limit the scaling range of $|t| \geq 0.01$. Therefore, an improved surface preparation is required to enlarge the scaling range in t which would then open a possibility to separate the corrections to scaling.

ACKNOWLEDGMENTS

We are indebted to R. Dennert, who recorded the data sets with the Faraday cup instrument. This work has been supported by the Deutsche Forschungsgemeinschaft through Grant No. SFB338.

* Present address: Physikalisches Institut der Universität Würzburg EPII, Am Hubland, D-97074 Würzburg, Germany.

[1] M. Schick, Prog. Surf. Sci. **11**, 245 (1981).
[2] C. Rottman, Phys. Rev. B **24**, 1482 (1981).
[3] W.N. Unertl, Comments Condens. Matter Phys. **12**, 289 (1986).
[4] E. Bauer, in *Structure and Dynamics of Surfaces II*, edited by W. Schommers and P. von Blanckenhagen (Springer, New York 1987), Vol. 43 p. 115.
[5] B.N.J. Persson, Surf. Sci. Rep. **15**, 1 (1992).
[6] K. Binder and D.P. Landau, in *Molecule-Surface Interaction*, edited by K. Lawley (Wiley, New York 1989), p. 91.
[7] P. Piercy and H. Pfnür, Phys. Rev. Lett. **59**, 1124 (1987); H. Pfnür and P. Piercy, Phys. Rev. B **40**, 2515 (1989).
[8] M. Sokolowski and H. Pfnür, Phys. Rev. Lett. **63**, 183 (1989).
[9] M. Sokolowski, H. Pfnür, and M. Lindroos, Surf. Sci. **278**, 87 (1992).
[10] A. Aharony and M. E. Fisher, Phys. Rev. B **27**, 4394 (1983).
[11] For example, P.M. Horn, R.J. Birgeneau, P. Heiney, and E.M. Hammonds, Phys. Rev. Lett. **41**, 961 (1978).
[12] For example, D.T. Keane, P.A. Bancel, J.L. Jordan-Sweet, G.A. Held, A. Mak, and R.L. Birgeneau, Surf. Sci. **250**, 250 (1991); E.G. McRae, T.M. Buck, and G.H. Wheatley, Phys. Rev. B **36**, 2341 (1987); D.E. Clark, W.N. Unertl, and P. Kleban, *ibid.* **34**, 4379 (1986).
[13] For example, M. Sandhoff, H. Pfnür, and H.-E. Everts, Surf. Sci. **280**, 185 (1993).
[14] H. Schlichting and D. Menzel, Surf. Sci. **285**, 209 (1993).
[15] U. Scheithauer, G. Meyer, and M. Henzler, Surf. Sci. **178**, 441 (1986).
[16] R. Dennert, M. Sokolowski, and H. Pfnür, Surf. Sci. **271**, 1 (1992).
[17] T.-M. Lu and M.G. Lagally, Surf. Sci. **120**, 47 (1982).
[18] D. Heuer, T. Müller, H. Pfnür, and U. Köhler, Surf. Sci. **297**, L61 (1993).
[19] D. Jürgens, G. Held, and H. Pfnür, Surf. Sci. **303**, 77 (1994).

[20] D. Heuer, T. Müller, H. Pfnür, and U. Köhler (unpublished)
[21] M.E. Fisher, Phys. Rev. **176**, 257 (1968).
[22] H.E. Stanley, *Introduction to Phase Transitions and Critical Phenomena* (Oxford University Press, London, 1971); L.D. Roelofs, Appl. Surf. Sci. **11/12**, 425 (1982).
[23] M.E. Fisher, J. Math. Phys. **5**, 944 (1964).
[24] ξ values defined in this way are larger by a factor of π with respect to the common definition, e.g., used in Refs. 7, 8, and 40.
[25] N.C. Bartelt, T.L. Einstein and L.D. Roelofs, Phys. Rev. B **32**, 2993 (1985).
[26] A.D. Bruce, J. Phys. C **14**, 193 (1981).
[27] V. Privman, P. C. Hohenberg, and A. Aharony, *Phase Transitions and Critical Phenomena*, edited by C. Domb and J.L. Lebowitz (Academic Press, London, 1991), Vol. 14, p. 1.
[28] J.L. Cardy, M. Nauenberg, and D.J. Scalapino, Phys. Rev. B **22**, 2560 (1980).
[29] N.C. Bartelt, T.L. Einstein, and L.D. Roelofs, Phys. Rev. B **35**, 1776 (1987).
[30] S. Uremovic, G. Held, M. Sokolowski, H. Pfnür, and D. Menzel (unpublished).
[31] F.Y. Wu, Rev. Mod. Phys. **54**, 235 (1982).
[32] For the recording of integrated intensities versus temperature at the $p(2\times2)$-O phase transition the integration area of the Faraday cup was 0.6% of the surface Brillouin zone (Ref. 7) and was thus approximately larger by a factor of 2 than in the present work.
[33] S.R. Kelemen and T.E. Fischer, Surf. Sci. **87**, 53 (1979).
[34] The relative contributions of the two peaks are dependent on the geometrical phase difference of electron waves scattered on adjacent terraces and the difference in scattering amplitudes. See also Ref. 9.
[35] P. Kleban, Surf. Sci. **103**, 542 (1981).
[36] M.E. Fisher and A.E. Ferdinand, Phys. Rev. Lett. **19**, 169 (1967).
[37] M.N. Barber, in *Phase Transitions and Critical Phenomena*, edited by C. Domb and J.L. Lebowitz (Academic Press, London 1983), Vol. 8, p. 145.
[38] L. D. Roelofs, A. R. Kortan, T. L. Einstein, and R. L. Park, Phys. Rev. Lett. **46**, 1465 (1981).
[39] L. Schwenger, C. Voges, M. Sokolowski, and H. Pfnür, Surf. Sci. (to be published).
[40] H. Pfnür and P. Piercy, Phys. Rev. B **41**, 582 (1990).
[41] A.D. Bruce, J. Phys. C **7**, 2089 (1975).
[42] C.A. Tracy and B.M. McCoy, Phys. Rev. B **12**, 368 (1975).
[43] P. Piercy, K. De'Bell, and H. Pfnür, Phys. Rev. B **45**, 1869 (1992).